INDERSCIENCE PUBLISHERS
Linking academia, business and industry through research

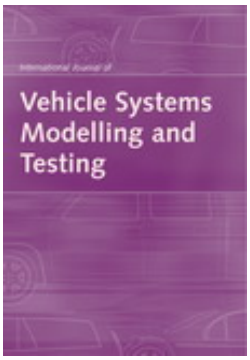

International Journal of Vehicle Systems Modelling and Testing

ISSN online: 1745-6444 - ISSN print: 1745-6436
https://www.inderscience.com/ijvsmt

Improved models of vehicle differential mechanisms using various approaches

Maksym Diachuk, Said M. Easa

DOI: 10.1504/IJVSMT.2023.10058372

Article History:
Received: 24 November 2021
Accepted: 05 December 2021
Published online: 20 August 2023

Improved models of vehicle differential mechanisms using various approaches

Maksym Diachuk and Said M. Easa*

Department of Civil Engineering,
Toronto Metropolitan University,
350 Victoria Street,
Toronto, Ontario, M5B2K3, Canada
Email: maksym.diachuk@torontomu.ca
Email: seasa@torontomu.ca
*Corresponding author

Abstract: The mathematical modelling of the branched automotive drivetrain is mainly based on various configurations of differential mechanisms (DM). This paper proposes variant math approaches for modelling DM's dynamics. The symmetric (open) DM is considered first. Two mathematical methods based on ordinary differential equation (ODE) and differential-algebraic equation (DEA) problems are applied. The asymmetric self-locking inter-axle differential with proportional friction moments is then considered. Three variants of the mathematical models for this DM type are represented. The linearised model uses the shortest description based on a previous step solution. Two other nonlinear models are formed by mixing with ODE and DAE approaches. The Simulink blocks for implementing developments were composed. The models were validated by comparing the results under the same conditions to prove their math coherence. The analysis of the proposed variants was carried out regarding structural complexity, usability, computational speed, and relative accuracy. Conclusions about their usability in drivetrain dynamics and active control were made.

Keywords: symmetric differential; self-locking differential; friction clutch; differential efficiency; differential simulink-model.

Reference to this paper should be made as follows: Diachuk, M. and Easa, S.M. (2023) 'Improved models of vehicle differential mechanisms using various approaches', *Int. J. Vehicle Systems Modelling and Testing*, Vol. 17, No. 2, pp.112–142.

Biographical notes: Maksym Diachuk, Research Associate (2016–2023), Department of Civil Engineering, Toronto Metropolitan University, Toronto, Canada. He worked as an Associate Professor at the Department of Operation and Maintenance of Machines, Mechanical Faculty, Prydniprovs'ka State Academy of Civil Engineering and Architecture, Ukraine (1998–2016) and as an Associate Professor, Department of Wheeled and Tracked Transport Means, Faculty of Mechanical Engineering, National Metallurgical Academy of Ukraine, Ukraine (2005–2014). He awarded the PhD in motor card and tractors, Kharkiv National Automobile and Highway University, Ukraine. His research interests include automotive systems, autonomous vehicles' dynamics and control, solid mechanics, numerical methods in engineering, mathematical statistics and probability, and simulation.

Said M. Easa is a Professor of Civil Engineering, Toronto Metropolitan University, Canada since 2000. He awarded PhD degree from University of California at Berkeley and BSc from Cairo University. He is a fellow of Canadian Academy of Engineering. He serves as Associated Editor of several international journals. He has numerous international, national, and local awards and honours from Canadian and U.S. organizations. His research interests include planning, design, operation, and management of transportation systems. He introduced innovative approaches for safer and more efficient transportation infrastructure, and has identified ways for improving the design of highway alignments, railway crossings, interchanges, intersections, and roundabouts.

1 Introduction

The DM is an integral part of the vehicle transmission, providing, in general, the redistribution of power between output shafts. The primary need for using differentials is caused by abolishing the power circulation in vehicle transmissions. Various designs and schemes of these mechanisms can improve the vehicle's performance depending on its operational purpose. Nevertheless, it is often impossible to simultaneously satisfy several contradicting criteria of high-performance properties using the classical mechanism. For example, applying the symmetric differential without internal friction ensures good steerability, high efficiency and prevents excessive tyre wear. However, it limits the vehicle passability owing to directing the primary power flow through a path with lower external resistance. Conversely, limited-slip differentials (LSD) ensure better passability but negatively affect steerability and increase tyre wear. These points are successfully resolved using ABS-based electronic control. Mechatronic DMs have gained importance owing to spreading a concept of redistributing torque by all wheels in AWD transmissions. Also, the unconditional advantages of a mechatronic differential can be referred to the fact that in the case of using single-motor electric traction, there is no additional need for controlling angular speeds of the same axle's wheels, as in the case of driving by a separate motor. Also, the torque redistribution can be organised with the sport differential technology.

The need for considering improved mathematical models of vehicle DMs is stipulated by several reasons: expansion of task range for 4-wheel and spatial vehicle models with dynamic redistribution of vertical reactions; analysis and modelling of complex powertrain schemes; actualisation of automatic transmission control issues associated with autonomous vehicles; intensification of technologies for intelligent distribution of traction forces; studies of transmission control algorithms using SIL/HIL modelling.

The purpose of this paper is to extend simulation models for basic types of vehicle DMs using various mathematical approaches for assessing the applicability and effectiveness of proposed models in issues of powertrain dynamics. Within the goals above, different methods for describing the DM dynamics are evaluated in terms of universality and complexity of models, ability to ensure high calculation speed, accuracy, integration into other and larger models of vehicle transmission, suitability for composing simulations and creating library components.

2 Literature review

Most studies in automotive differentials can be conditionally divided into issues of the modelling mechanisms themselves and studies considering differentials as an electronic control system component. Brumercik et al. (2015) evaluated the model of inter-wheel differential that engaged into a vehicle drivetrain model. The basic math model is based on power balance, including kinematic relations between three shafts. The reduced inertia coefficients are determined by comparing the unit's reduced kinetic energy with the kinetic energy of all the components. The system of three differential equations was composed for describing the mechanism state. The model does not consider efficiencies and other losses inside of the mechanism or changes of power flows.

Virlez et al. (2011) developed detailed models of TORSEN differentials using a flexible multibody simulation approach based on the nonlinear FEM. The prototype model was composed of several rigid and flexible bodies mainly constrained by flexible gear pair joints and contact conditions. Math equations formed a nonlinear differential-algebraic system solved using a Newton-Raphson method. The proposed model was engaged into an all-wheel-drive model, including shafts and tyres, to estimate torque redistribution by axles. The authors stated that the results were obtained with good accuracy.

Chen et al. (2017a) considered a new torque vectoring differential (TVD) based on a *Ravigneaux* gear set. This design was chosen for using the option of generating two different speed ratios with only one pair of the gear set. The equation system of mechanism dynamics consists of two parts, including Ravigneaux equations and symmetric differential equations combined in one DAE problem. Further, the model was engaged into the vehicle dynamics model composed using *SimulationX* software. Virtual tests were conducted to determine the effect of the proposed differential on vehicle manoeuvrability and steerability.

Chen et al. (2017b) considered a differential mechanism's original design for realising the torque vectoring concept. The new TVD system consists of gear sets, actuator, and control. The technique combines the inner gears that drive output shafts and outer gears connected to brakes. The math model is represented by dynamic equations of elements complemented by equations of kinematic constraints that compose the DAE problem. Any losses and efficiencies are neglected, and the power flow direction correspondingly. The sensitivity of design parameters was analysed, including the braking torques' adjustment and dimensions of gear sets.

Forstinger et al. (2015) developed a model of asymmetric differential. Two variants of differential design were considered, namely composed with conic and planetary gear sets. Math models are based on both dynamics and constraint equations. The model includes static friction for describing losses and limited-slip functionality. A method based on force-balancing for overcoming the simulation problems of discontinuity at zero angular speed was presented. Simulation studies showed high similarities with measurement data from a differential gear testbed.

Russo et al. (2016) proposed a new controllable differential based on the magnetorheological fluid to generate the locking torque. The differential state system is composed of the torque, power balance, and kinematic constraint equations. The double-controller, including the extended Kalman filter scheme, was designed to correct the

yaw moment. Modelling of the software and hardware in the loop was conducted with an experimental prototype.

Two models of differential mechanisms are represented in the Simulink library of Mathworks (2021a, 2021b). The *Open Differential* and *Limited Slip Differential* blocks are based on simplified differential equations of components' equilibrium supplemented by algebraic equations of kinematic constraints. The models consider the mechanical efficiencies (constant and load/speed-dependency), viscous losses, working temperature and are fully configurable. The main difference between the models is constant friction moment depending on the relative angular speed.

As noted, the research field of DM models is vast and can be conditionally divided into the following sectors: modelling and studying specific properties of a DM (Gadola and Chindamo, 2018; Morselli et al., 2006; Deur et al., 2010), vehicle dynamics with active differentials (Annicchiarico et al., 2014; Ji et al., 2011), torque redistribution systems (Jaafari and Shirazi, 2018), and development of control algorithms for improving vehicle steerability and passability (Assadian et al., 2008). Nevertheless, simplifications and assumptions are accepted in many studies, and the differential efficiency and operational modes are not considered. We also note that the authors rarely present simulation models, their validation, performance and model quality assessments, and comparison of different approaches, which somewhat reduces the reliability of the proposed models.

3 Symmetric differential mechanism

3.1 Schemes

The same axle wheels are often driven using a symmetric (open) differential, ensuring approximately equal redistributions of the carrier torque via the side gears on output shafts 1 and 2. This differential provides good steerability for a front-wheel-drive (FWD) vehicle due to the absence of internal friction. Still, it reduces vehicle passability since the power flow runs over the wheel with worse tyre-road adhesion. It can be compensated by activating a brake on such a wheel to augment the moment of internal resistance.

The symmetric DM shown in Figure 1 is combined with the final drive. Shaft 3 is accepted as the input because the torque goes straight from a gearbox to the wheels most operating time. The ring gear of the radius R_0 joined with the differential carrier composes a final drive conic pair with the shaft pinion of radius r_3, the quotient of which gives the algebraic (module) ratio $g_F = R_F / r_F$ unlike the quotient of their angular speeds $i_F = \pm g_F$ due to the clockwise/counterclockwise rotation of the ring and pinion gear, respectively. As this DM divides the torque between the same axle wheels, the side gear radii R_1 and R_2 are equal. The satellite with a radius r_s works like a parasite gear. Nevertheless, it affects the internal inertial losses depending on the radii ratio of the satellite and side gear. Thus, the ratio from $k = 1,2$ side gear to the satellite yields $g_{ks} = r_s / R_k$.

Figure 1 Schemes of symmetric differential mechanism: (a) kinematic; (b) side gears and satellites and (c) final drive (see online version for colours)

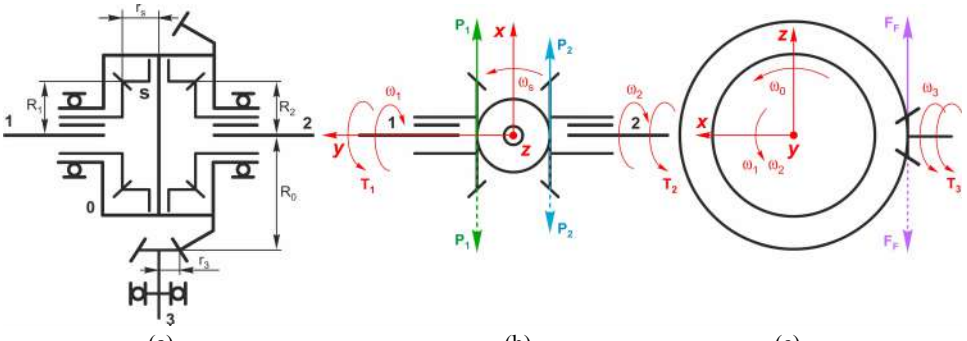

(a) (b) (c)

3.2 Differential kinematics

Introducing the designations following the mechanism scheme in Figure 1(a), it can be written

$$\boldsymbol{\omega} = \begin{pmatrix} \omega_0 & \omega_1 & \omega_2 & \omega_3 & \omega_s \end{pmatrix}^T, \ \boldsymbol{\omega}_D = \begin{pmatrix} \omega_1 \\ \omega_2 \end{pmatrix}, \ \boldsymbol{\varepsilon}_D = \frac{d\boldsymbol{\omega}_D}{dt} = \begin{pmatrix} \varepsilon_1 \\ \varepsilon_2 \end{pmatrix} \tag{1}$$

where ω_0, ω_1, ω_2, ω_3, ω_s – angular velocities of the carrier, left-side gear, right-side gear, final drive pinion, and satellite, respectively; $\boldsymbol{\omega}$ – vector of absolute angular speeds of differential mechanism; $\boldsymbol{\omega}_D$, $\boldsymbol{\varepsilon}_D$ – vectors of driving axles' angular speeds and accelerations, correspondingly.

The basic kinematic relations between the components of a vehicle DM may be represented with the well-known Willis formula

$$i_{12}^{(0)} = \frac{\omega_1 - \omega_0}{\omega_2 - \omega_0} = \frac{\omega_1^{(0)}}{\omega_2^{(0)}} = -\frac{z_s}{z_1}\frac{z_2}{z_s} = \frac{i_{1s}^{(0)}}{i_{2s}^{(0)}} = -\frac{z_2}{z_1} = -g_{12} = \frac{-g_{1s}}{g_{2s}} \tag{2}$$

where $i_{12}^{(0)}$, g_{12} – kinematic ratio and its module between the input shaft 1 and the output shaft 2 at the stopped carrier, respectively; z_1, z_2, z_s – teeth number for the left and right side gears, and satellite, respectively; $i_{1s}^{(0)}$, g_{1s}, $i_{2s}^{(0)}$, g_{2s} – kinematic ratios (and their modules) between the input shaft 1, input shaft 2, and the satellite at the stopped carrier, respectively.

Axle 1 positive rotation causes the negative satellite rotation, and conversely, the same signs for the side gear and satellite are kept in the case of the driving axle 2. Thus

$$i_{1s}^{(0)} = -g_{1s} = -\frac{z_s}{z_1}, \ i_{2s}^{(0)} = g_{2s} = \frac{z_s}{z_2} \tag{3}$$

After determining the kinematic ratio $i_{12}^{(0)}$, the carrier angular speed may be derived by angular speeds ω_1, ω_2 of axles 1, 2, respectively.

$$\omega_0 = \frac{\omega_1 - i_{12}^{(0)}\omega_2}{1 - i_{12}^{(0)}} = \frac{\omega_1 + g_{12}\omega_2}{1 + g_{12}} \tag{4}$$

For the inter-wheel DM depicted in Figure 1, the kinematic ratio $i_{12}^{(0)} = -1$, and thus, the carrier and satellite angular speeds may be derived using equations (3) and (4)

$$\omega_0 = (\omega_1 + \omega_2)/2\,,\ \omega_s = (\omega_2 - \omega_1)/(2g_{2s}) \tag{5}$$

Thus, all the angular speeds of $\boldsymbol{\omega}_D$ vector may be found by the customary kinematic conditions equations (3) and (5) and a couple of angular speeds of $\boldsymbol{\omega}$. Denote the auxiliary matrices

$$\boldsymbol{g}_D = \frac{1}{2}\begin{pmatrix} 1 & 1 \\ 2 & 0 \\ 0 & 2 \\ g_F & g_F \\ -1/g_{2s} & 1/g_{2s} \end{pmatrix},\ \boldsymbol{g}_H = \frac{1}{2}\begin{pmatrix} 0 & 0 \\ 1 & 1 \\ 1 & 1 \\ 0 & 0 \\ 0 & 0 \end{pmatrix},\ \boldsymbol{\omega}_H = \omega_0 \begin{pmatrix} 0 \\ 1 \\ 1 \\ 0 \\ 0 \end{pmatrix} \tag{6}$$

where $\boldsymbol{g}_D$ – matrix of kinematic ratios of the differential links relative to shafts 1 and 2, $\boldsymbol{g}_H$ – matrix of gear ratios relative to supports of rotating links, $\boldsymbol{\omega}_H$ – vector of rotational speeds of support details.

Almost all the differential components have stationary supports with no rotation except for the side gears that are usually connected via a sleeve bearing with the carrier body. Thus, the vector $\boldsymbol{\omega}_H$ specifies the angular velocities of supports of corresponding details. Then, the absolute and relative angular speeds are given by

$$\boldsymbol{\omega} = \boldsymbol{g}_D\boldsymbol{\omega}_D\,,\ \boldsymbol{\omega}_H = \boldsymbol{g}_H\boldsymbol{\omega}_D\,,\ \boldsymbol{\omega}_r = \boldsymbol{\omega} - \boldsymbol{\omega}_H = (\boldsymbol{g}_D - \boldsymbol{g}_H)\boldsymbol{\omega}_D \tag{7}$$

The angular accelerations corresponding to the mechanism details may be obtained by differentiating equations (1) and (5), which gives two basic and additional important relations

$$\varepsilon_3 = \varepsilon_0 i_3 = \pm\varepsilon_0 g_3\,,\ \varepsilon_0 = \frac{\varepsilon_1 + \varepsilon_2}{2}\,,\ \varepsilon_s = \frac{\varepsilon_2 - \varepsilon_1}{2g_{2s}} \tag{8}$$

3.3 Variant 1: absolute and relative balance of DM

3.3.1 Differential dynamics

To model the DM dynamics, consider the case of direct power flow from the final drive's pinion shaft to wheel axles. For each side gear $(k = 1,2)$

$$I_k\varepsilon_k = n_s P_k R_k - G_k - L_k + T_k \tag{9}$$

where I_k – side gear inertia, P_k – driving force in the gearing contact between side gear and satellites, G_k – moment of gearing losses, L_k – moment of viscous losses, T_k – external axle torque, n_s – number of satellites.

The gearing losses may be considered with efficiency coefficient η_{kG} relative to the internal interaction torque $P_k R_k$

$$I_k \varepsilon_k = n_s P_k R_k \eta_{kG} - L_k + T_k \tag{10}$$

Thus, the driving torque on a side gear may be derived as

$$-n_s P_k R_k = -\frac{I_k}{\eta_{kG}} \varepsilon_k - \frac{L_k}{\eta_{kG}} + \frac{T_k}{\eta_{kG}} \tag{11}$$

The carrier dynamics equation

$$I_0 \varepsilon_0 = P_F R_F - G_F - B_0 - L_0 - n_s \sum_k P_k R_k + \sum_k L_k \tag{12}$$

where I_0 – carrier inertia, P_F – driving contact force between the final drive's ring and pinion gears, G_F – moment of final drive gearing losses, B_0 – moment of bearing losses in carrier supports, L_0 – moment of viscous carrier losses.

Note that usually, a side gear does not have its bearing (Figure 1(a)), using a carrier's internal surface for sliding. Consequently, the viscous losses L_k between these counter-bodies appear when there is a difference in their angular speeds. Thus, the influence from the side gear slip also spreads on a carrier. Introducing gearing and bearing efficiencies η_{FG}, η_{0B}, respectively, and substituting equation (11), based on the previous expression obtain

$$I_0 \varepsilon_0 \eta_{0B} + \sum_k \frac{I_k}{\eta_{kG}} \varepsilon_k = P_F R_F \eta_{FG} \eta_{0B} - L_0 + \sum_k \frac{T_k}{\eta_{kG}} - \sum_k \left(\frac{1}{\eta_{kG}} - 1 \right) L_k \tag{13}$$

The sum of viscous components L_k in equation (13) expresses the losses caused by a specific power circulation between the carrier and side gears and reduced to the sliding moments. On the one hand, the carrier drives a side gear; on the other hand, a side gear may rotate faster than the carrier, returning some power through the liquid friction. Denote

$$\eta_{kL} = \left(\frac{1}{\eta_{kG}} - 1 \right) = \frac{1 - \eta_{kG}}{\eta_{kG}} \tag{14}$$

Then, considering the sum mentioned and kinematic relation of equation (7)

$$\sum_k \left(\frac{1}{\eta_{kG}} - 1 \right) L_k = \sum_k \eta_{kL} l_k \left(\omega_k - \omega_0 \right) = \frac{1}{2} \left(\eta_{1L} l_1 - \eta_{2L} l_2 \right) \left(\omega_1 - \omega_2 \right) \tag{15}$$

where l_k – linear coefficient of the side gear's viscous resistance.

Analysing equation (15), it can be observed first that in the case of equal efficiencies $\eta_{1G} = \eta_{2G}$ and at the same time, the specific viscosities $l_1 = l_2$, the equation (15) gives zero, as well as for the case of equal angular speeds $\omega_1 = \omega_2$. If, for instance, $\eta_{1L} l_1 > \eta_{2L} l_2$, meaning the increased resistance on the side gear 1, the positive difference $\omega_1 - \omega_2 > 0$ gives the positive loss to be subtracted from the carrier torque. If at the same

condition $\omega_1 - \omega_2 < 0$, the loss becomes negative but, considering its deduction in equation (13), implies redistributing the power over the side gear 2. The same reasoning is for the case of the opposite side gear.

According to the coordinate system accepted for the DM with the final drive, the ring gear may be located left- or rightward relative to the pinion. The design solution affects the ratio sign, whether the pinion shaft would rotate clockwise or counterclockwise. Any variant uses the same equation of the pinion balance

$$I_3\varepsilon_3 = T_3 - B_3 - L_3 - P_F r_F \tag{16}$$

where I_3 – inertia of the final drive pinion with its shaft; B_3, L_3 – moments of pinion shaft bearing and viscous losses, respectively, r_F – conditional pinion radius (Figure 1(a)).

Introducing bearing effectiveness η_{3B}, multiplying the equation (16) on g_F, substituting $R_F = r_F g_F$, replacing the angular acceleration ε_3 of the pinion shaft with relation from equation (8), derive the carrier drive torque

$$P_F R_F = T_3 g_F \eta_{3B} - L_3 g_F - \frac{I_3 g_F^2}{2}\eta_{3B}\varepsilon_1 - \frac{I_3}{2} g_F^2 \eta_{3B}\varepsilon_2 \tag{17}$$

Note that the issue of the carrier ring location can be easily solved by a sign of g_F, thus, for the case depicted in Figure 1(a), g_F must be negative.

The first equation of the differential state may be derived by combining equations (8), (13), and (17) that after simplifying is reduced to the form

$$I_{1\Sigma}\varepsilon_1 + I_{2\Sigma}\varepsilon_2 = T_\Sigma - L_\Sigma \tag{18}$$

where the total moments of inertias $I_{1\Sigma}$, $I_{2\Sigma}$, torque T_Σ, and viscous resistance L_Σ, respectively are

$$I_{\Sigma 1} = \frac{I_0}{2\eta_{FG}} + \frac{I_1}{\eta_{FG}\eta_{0B}\eta_{1G}} + \frac{I_3 g_F^2}{2}\eta_{3B},\ I_{2\Sigma} = \frac{I_0}{2\eta_{FG}} + \frac{I_2}{\eta_{FG}\eta_{0B}\eta_{2G}} + \frac{I_3}{2} g_F^2 \eta_{3B} \tag{19}$$

$$T_\Sigma = \frac{1}{\eta_{FG}\eta_{0B}}\left(\frac{T_1}{\eta_{1G}} + \frac{T_2}{\eta_{2G}}\right) + T_3 g_F \eta_{3B},\quad L_\Sigma = \frac{1}{\eta_{FG}\eta_{0B}}\left(L_0 + \eta_{1L}L_1 + \eta_{2L}L_2\right) + L_3 g_F \tag{20}$$

Thereby, the torque T_3 and loss L_3 in the last expressions for T_Σ and L_Σ change their signs automatically according to the driving speed ω_3 sign. In this way, equation (18) fully reflect the power balance of the mechanism.

Unlike the adopted principle at considering the symmetric differential's power balance, assume that satellite contact forces P_1 and P_2 maybe different, which allows taking the satellite inertia into account. Thus, the force equation of a satellite equilibrium yields

$$I_s\varepsilon_s = \left(P_1 - P_2\right) r_s - L_s \tag{21}$$

where I_s – satellite inertia, L_s – moment of viscous satellite losses.

The second equation of the differential state may be derived by multiplying equation (21) on n_s, combining equations (8), (10), and (21), and substituting $r_s = R_2 g_{2s} = R_1 g_{2s}$, which after simplifying gets the form

$$I_{2S}\varepsilon_2 - I_{1S}\varepsilon_1 = T_S - L_S \tag{22}$$

where the subtractive moments of inertias I_{1S}, I_{2S}, torque T_S, and viscous resistance L_S (large index), are, respectively

$$I_{1s} = \frac{I_1}{\eta_{1G}} + \frac{n_s I_s}{2g_{2s}^2},\ I_{2s} = \frac{I_2}{\eta_{2G}} + \frac{n_s I_s}{2g_{2s}^2},\ T_S = \frac{T_2}{\eta_{2G}} - \frac{T_1}{\eta_{1G}},\ L_S = \frac{L_2}{\eta_{2G}} - \frac{L_1}{\eta_{1G}} + \frac{n_s L_s}{g_{2s}} \tag{23}$$

Note that equations (22) and (23) do not contain parameters and efficiencies from the carrier and final drive and, in this way, describe the relative power balance between side gear shafts. Consequently, there are two equations (18) and (22) for the mechanism with two degrees of freedom, enough for linking the kinematic and dynamic parameters. Consider the parts of these equations separately to perform in the vector-matrix form

$$\begin{pmatrix} I_{\Sigma 1} & I_{2\Sigma} \\ -I_{1S} & I_{2S} \end{pmatrix} \begin{pmatrix} \varepsilon_1 \\ \varepsilon_2 \end{pmatrix} = \begin{pmatrix} T_\Sigma \\ T_S \end{pmatrix} - \begin{pmatrix} L_\Sigma \\ L_S \end{pmatrix} \tag{24}$$

3.3.2 Matrix of inertia

The matrix $\boldsymbol{I}_D$ of the inertia coefficients is nonsingular, therefore invertible at any combinations of rotating components inertias except for the case they equal zero.

$$\boldsymbol{I}_D = \begin{pmatrix} I_{\Sigma 1} & I_{2\Sigma} \\ -I_{1S} & I_{2S} \end{pmatrix} = \begin{pmatrix} \boldsymbol{I}_\Sigma \\ \boldsymbol{I}_S \end{pmatrix} \tag{25}$$

where $\boldsymbol{I}_\Sigma$, $\boldsymbol{I}_S$ – row-vectors of total and subtractive inertias, respectively.

Introducing the vector $\boldsymbol{I}$ of the differential mechanism inertias and matrices $\boldsymbol{\eta}_\Sigma$, $\boldsymbol{\eta}_S$ of combined kinematic and efficiency influences, it can be expressed as

$$\boldsymbol{I} = \begin{pmatrix} I_0 \\ I_1 \\ I_2 \\ I_3 \\ I_s \end{pmatrix},\ \boldsymbol{\eta}_\Sigma = \begin{pmatrix} \frac{1}{2\eta_{FG}} & \frac{1}{2\eta_{FG}} \\ \frac{1}{\eta_{FG}\eta_{0B}\eta_{1G}} & 0 \\ 0 & \frac{1}{\eta_{FG}\eta_{0B}\eta_{2G}} \\ \frac{g_F^2\eta_{3B}}{2} & \frac{g_F^2\eta_{3B}}{2} \\ 0 & 0 \end{pmatrix},\ \boldsymbol{\eta}_S = \begin{pmatrix} 0 & 0 \\ -\frac{1}{\eta_{1G}} & 0 \\ 0 & \frac{1}{\eta_{2G}} \\ 0 & 0 \\ -\frac{n_s}{2g_{2s}^2} & \frac{n_s}{2g_{2s}^2} \end{pmatrix} \tag{26}$$

Then

$$\boldsymbol{I}_\Sigma = \boldsymbol{I}^T\boldsymbol{\eta}_\Sigma,\ \boldsymbol{I}_S = \boldsymbol{I}^T\boldsymbol{\eta}_S \tag{27}$$

3.3.3 Torques

Introducing designations for influences of external torques, then

$$\boldsymbol{T}=\begin{pmatrix}T_1\\T_2\\T_3\end{pmatrix},\ \boldsymbol{\eta}_T=\begin{pmatrix}\dfrac{1}{\eta_{FG}\eta_{0B}\eta_{1G}} & \dfrac{1}{\eta_{FG}\eta_{0B}\eta_{2G}} & \eta_{3B}\\ -\dfrac{1}{\eta_{1G}} & \dfrac{1}{\eta_{2G}} & 0\end{pmatrix},\ \boldsymbol{g}=\begin{pmatrix}1\\1\\g_F\end{pmatrix},\ \boldsymbol{g}_T=diag\left(\boldsymbol{g}\right) \tag{28}$$

where $\boldsymbol{T}$ – vector of external torques on corresponding shafts, $\boldsymbol{\eta}_T$ – efficiency matrix of power losses, $\boldsymbol{g}$ – vector of ratios by corresponding axles. Then, the vector of torques may be expressed as

$$\begin{pmatrix}T_\Sigma\\T_S\end{pmatrix}=\boldsymbol{\eta}_T\boldsymbol{g}_T\boldsymbol{T} \tag{29}$$

3.3.4 Viscous losses

Viscous losses may be represented by a linear dependency, where the moment is proportional to the relative angular speed of rotating detail and being weighed by a coefficient l_k. Combining all the viscous losses from equation (24), it can be expressed in matrix form as

$$\boldsymbol{L}=\begin{pmatrix}L_0\\L_1\\L_2\\L_3\\L_s\end{pmatrix},\ \boldsymbol{l}=diag\begin{pmatrix}l_0\\l_1\\l_2\\l_3\\l_s\end{pmatrix},\ \boldsymbol{g}_L=diag\begin{pmatrix}1\\\boldsymbol{g}\\\dfrac{n_s}{g_{2s}}\end{pmatrix},$$

$$\boldsymbol{\eta}_L=\begin{pmatrix}\dfrac{1}{\eta_{FG}\eta_{0B}} & \dfrac{\eta_{1L}}{\eta_{FG}\eta_{0B}\eta_{1G}} & \dfrac{\eta_{2L}}{\eta_{FG}\eta_{0B}\eta_{2G}} & 1 & 0\\ 0 & -\dfrac{1}{\eta_{1G}} & \dfrac{1}{\eta_{2G}} & 0 & 1\end{pmatrix} \tag{30}$$

where $\boldsymbol{L}$ – vector of moments of viscous losses over all the differential's components, $\boldsymbol{l}$ – diagonal matrix of viscous moments' coefficients, $\boldsymbol{g}_L$ – ratio matrix for reducing the viscous resistances, $\boldsymbol{\eta}_L$ – efficiency matrix of viscous influence.

Thus, the viscous losses in all the elements of the differential mechanism

$$\boldsymbol{L}=\boldsymbol{l}\boldsymbol{\omega}_r=\boldsymbol{l}\left(\boldsymbol{\omega}_D-\boldsymbol{\omega}_H\right) \tag{31}$$

Then, the viscous part of equation (24), considering equations (7) and (31), is given by

$$\begin{pmatrix}L_\Sigma\\L_S\end{pmatrix}=\boldsymbol{\eta}_L\boldsymbol{g}_L\boldsymbol{l}\left(\boldsymbol{g}_D-\boldsymbol{g}_H\right)\boldsymbol{\omega}_D \tag{32}$$

Finally, the system of dynamic balance for the symmetric differential mechanism may be represented in the vector-matrix form as follows

$$\boldsymbol{\varepsilon}_D = \boldsymbol{I}_D^{-1}\left(\boldsymbol{\eta}_T \boldsymbol{g}_T \boldsymbol{T} - \boldsymbol{\eta}_L \boldsymbol{g}_L \boldsymbol{l}\left(\boldsymbol{g}_D - \boldsymbol{g}_H\right)\boldsymbol{\omega}_D\right) \tag{33}$$

Equation (33) may be rewritten in a state-space form as

$$\dot{\boldsymbol{\omega}}_D = \boldsymbol{A}\boldsymbol{\omega}_D + \boldsymbol{B}\boldsymbol{u} \tag{34}$$

where

$$\boldsymbol{A} = -\boldsymbol{I}_D^{-1}\boldsymbol{\eta}_L \boldsymbol{g}_L \boldsymbol{l}\left(\boldsymbol{g}_D - \boldsymbol{g}_H\right),\ \boldsymbol{B} = \boldsymbol{I}_D^{-1}\boldsymbol{\eta}_T \boldsymbol{g}_T,\ \boldsymbol{u} = \boldsymbol{T}$$

3.3.5 Direct and reverse power flows

Note that the power flow may be considered as direct when the power at the mechanism entrance exceeds the total output power. Thus

$$\left|T_3\omega_3\right| > \left|T_1\omega_1 + T_2\omega_2\right| \tag{35}$$

Here the output power flows $T_1\omega_1$, $T_2\omega_2$ are algebraically taken since they can only redistribute the power between each other and may not affect the driving flow $T_3\omega_3$. Assuming that the mechanism's direct and reverse efficiencies are approximately equal, the condition of detecting the reverse power flow is

$$\left|T_1\omega_1 + T_2\omega_2\right| \geq \left|T_3\omega_3\right| \tag{36}$$

There is a particular power gap inside these specified statements meaning a lack of power to overcome the internal resistance stipulated by the total losses. Thus, when the external driving and resisting power are almost equal and no motion of details, the mechanism turns out to be insensitive.

The mechanism mechanical efficiency may be estimated as follows

$$\eta_D = \eta_{3B}\eta_{FG}\eta_{0B}\frac{\eta_{1G} + \eta_{1G}}{2} \tag{37}$$

These coefficients do not depend on angular speed and represent the minimum internal losses overlapped by the driving torque at the start.

In the case of driving the mechanism from side gears, the system of equations may be derived in the same style with minor differences stipulated by shifting the order of internal losses. The structure and components match equations (26), (28), and (30). The basic formulas are represented to avoid excessive derivations, as follows

$$\boldsymbol{\eta}_\Sigma = \begin{pmatrix} \frac{\eta_{0B}}{2} & \frac{\eta_{0B}}{2} \\ \eta_{1G}\eta_{0B} & 0 \\ 0 & \eta_{0B}\eta_{2G} \\ \frac{g_F^2}{2\eta_{FG}} & \frac{g_F^2}{2\eta_{FG}} \\ 0 & 0 \end{pmatrix},\ \boldsymbol{\eta}_S = \begin{pmatrix} 0 & 0 \\ -\eta_{1G} & 0 \\ 0 & \eta_{2G} \\ 0 & 0 \\ -\frac{n_s}{2g_{2s}^2} & \frac{n_s}{2g_{2s}^2} \end{pmatrix} \tag{38}$$

$$\boldsymbol{\eta}_T = \begin{pmatrix} \eta_{1G}\eta_{0B} & \eta_{2G}\eta_{0B} & \dfrac{1}{\eta_{FG}\eta_{3B}} \\ -\eta_{1G} & \eta_{2G} & 0 \end{pmatrix},\ \boldsymbol{\eta}_L = \begin{pmatrix} 1 & \eta_{1L} & \eta_{2L} & \dfrac{1}{\eta_{FG}\eta_{3B}} & 0 \\ 0 & -\eta_{1G} & \eta_{2G} & 0 & 1 \end{pmatrix} \tag{39}$$

where $\eta_{kL} = \eta_{0B}\eta_{kG} - 1$, for $k = 1,2$.

3.4 Variant 2: model with kinematic constraints

In this variant, the dynamics equations of all the DM components are considered separately combined with imposed kinematic constraints.

3.4.1 Direct power flow

Collecting equations (10), (13), (17), and (21) and rewriting them as a system, then

$$\begin{cases} I_0\varepsilon_0 = P_F R_F \eta_{FG} - \dfrac{n_s P_1 R_1}{\eta_{0B}} - \dfrac{n_s P_2 R_2}{\eta_{0B}} - \dfrac{L_0}{\eta_{0B}} + \dfrac{L_1}{\eta_{0B}} + \dfrac{L_2}{\eta_{0B}} \\ I_1\varepsilon_1 = n_s P_1 R_1 \eta_{1G} - L_1 + T_1 \\ I_2\varepsilon_2 = n_s P_2 R_2 \eta_{2G} - L_2 + T_2 \\ I_3\varepsilon_3 g_F = -\dfrac{P_F R_F}{\eta_{3B}} \dfrac{L_3 g_F}{\eta_{3B}} + T_3 g_F \\ \dfrac{n_s I_s}{g_{2s}}\varepsilon_s = n_s P_1 R_1 - n_s P_2 R_2 - \dfrac{n_s L_s}{g_{2s}} \end{cases} \tag{40}$$

The variables of equation (40) may be represented using vector-matrix decomposition. Thus, denote

$$\boldsymbol{\varepsilon} = \begin{pmatrix} \varepsilon_0 \\ \varepsilon_1 \\ \varepsilon_2 \\ \varepsilon_3 \\ \varepsilon_s \end{pmatrix},\ \boldsymbol{I} = diag\begin{pmatrix} I_0 \\ I_1 \\ I_2 \\ I_3 \\ I_s \end{pmatrix},\ \boldsymbol{T} = \begin{pmatrix} 0 \\ T_1 \\ T_2 \\ T_3 \\ 0 \end{pmatrix},\ \boldsymbol{M} = \begin{pmatrix} M_0 \\ M_1 \\ M_2 \end{pmatrix} = \begin{pmatrix} P_F R_F \\ n_s P_1 R_1 \\ n_s P_2 R_2 \end{pmatrix},\ \boldsymbol{g} = diag\begin{pmatrix} 1 \\ 1 \\ 1 \\ g_F \\ \dfrac{n_s}{g_{2s}} \end{pmatrix} \tag{41}$$

where $\boldsymbol{M}$ – vector of unknown internal moments.

The efficiency matrices corresponding to internal mechanical $\boldsymbol{\eta}_M$ and viscous $\boldsymbol{\eta}_L$ moments are

$$\boldsymbol{\eta}_M = \begin{pmatrix} -\eta_{FG} & \dfrac{1}{\eta_{0B}} & \dfrac{1}{\eta_{0B}} \\ 0 & -\eta_{1G} & 0 \\ 0 & 0 & -\eta_{2G} \\ \dfrac{1}{\eta_{3B}} & 0 & 0 \\ 0 & -1 & 1 \end{pmatrix}, \quad \boldsymbol{\eta}_L = \begin{pmatrix} \dfrac{1}{\eta_{0B}} & \dfrac{-1}{\eta_{0B}} & \dfrac{-1}{\eta_{0B}} & 0 & 0 \\ 0 & 1 & 0 & 0 & 0 \\ 0 & 0 & 1 & 0 & 0 \\ 0 & 0 & 0 & \dfrac{1}{\eta_{3B}} & 0 \\ 0 & 0 & 0 & 0 & 1 \end{pmatrix} \tag{42}$$

Then, equation (42) in the vector-matrix form

$$\boldsymbol{Ig\varepsilon} = \boldsymbol{gT} - \boldsymbol{\eta}_M \boldsymbol{M} - \boldsymbol{\eta}_L \boldsymbol{gL} \tag{43}$$

The vector $\boldsymbol{L}$ of viscous loss may be expressed as

$$\boldsymbol{L} = \boldsymbol{l}\left(\boldsymbol{\omega} - \boldsymbol{\omega}_H\right) = \boldsymbol{l}\boldsymbol{e}_\omega \boldsymbol{\omega} \tag{44}$$

where

$$\boldsymbol{e}_\omega = \begin{pmatrix} 1 & 0 & 0 & 0 & 0 \\ -1 & 1 & 0 & 0 & 0 \\ -1 & 0 & 1 & 0 & 0 \\ 0 & 0 & 0 & 1 & 0 \\ 0 & 0 & 0 & 0 & 1 \end{pmatrix}$$

Since the vector $\boldsymbol{M}$ contains three unknown variables and considering equations (44), (43) may be represented as

$$\boldsymbol{Ig\varepsilon} + \boldsymbol{\eta}_M \boldsymbol{M} = \boldsymbol{gT} - \boldsymbol{\eta}_L \boldsymbol{gle}_\omega \boldsymbol{\omega} \tag{45}$$

Thus, equation (45) consists of five equations with eight unknowns $\left(\boldsymbol{\varepsilon}^T \quad \boldsymbol{M}^T\right)$. Such a discrepancy may be compensated with algebraic constraint equations. The kinematic links are based on relations of equation (8)

$$\begin{cases} \omega_0 = \left(\omega_1 + \omega_2\right)/2 \\ \omega_3 = g_F \omega_0 \\ \omega_s = \left(\omega_2 - \omega_1\right)/\left(2g_{2s}\right) \end{cases} \tag{46}$$

Differentiating the last system and denoting $\boldsymbol{g}_\omega$, the system of additional algebraic constraints takes the form

$$\boldsymbol{g}_\omega = \begin{pmatrix} 2 & -1 & -1 & 0 & 0 \\ g_F & 0 & 0 & -1 & 0 \\ 0 & 1 & -1 & 0 & 2g_{2s} \end{pmatrix}, \quad \boldsymbol{g}_\omega \boldsymbol{\varepsilon} = \boldsymbol{Z}_{3,1} \tag{47}$$

where $\boldsymbol{Z}_{3,1}$ – zero vector of *3x1* dimension. Designate new vectors as

$$\dot{\boldsymbol{x}} = \begin{pmatrix} \boldsymbol{\varepsilon} \\ \boldsymbol{M} \end{pmatrix},\ \boldsymbol{T}_D = \begin{pmatrix} \boldsymbol{T} \\ \boldsymbol{Z}_{3,1} \end{pmatrix},\ \boldsymbol{x} = \begin{pmatrix} \boldsymbol{\omega} \\ \boldsymbol{K} \end{pmatrix} \tag{48}$$

where $\boldsymbol{K}$ – vector of internal moments' integral.

And block matrices as

$$\boldsymbol{g}_T = \begin{pmatrix} \boldsymbol{g} & \boldsymbol{Z}_{5,3} \\ \boldsymbol{Z}_{3,5} & \boldsymbol{Z}_{3,3} \end{pmatrix},\ \boldsymbol{I}_D = \begin{pmatrix} \boldsymbol{Ig} & \boldsymbol{\eta}_M \\ \boldsymbol{g}_\omega & \boldsymbol{Z}_{3,3} \end{pmatrix},\ \boldsymbol{g}_L = \begin{pmatrix} \boldsymbol{\eta}_L \boldsymbol{gle}_\omega & \boldsymbol{Z}_{5,3} \\ \boldsymbol{Z}_{3,5} & \boldsymbol{Z}_{3,3} \end{pmatrix} \tag{49}$$

where $\boldsymbol{Z}_{m,n}$ – zero matrix of $m \times n$ dimension. Consequently, the system combining equations (48) and (49) becomes

$$\boldsymbol{I}_D \dot{\boldsymbol{x}} = \boldsymbol{g}_T \boldsymbol{T}_D - \boldsymbol{g}_L \boldsymbol{x} \tag{50}$$

which can be represented in the state-space form

$$\dot{\boldsymbol{x}} = \boldsymbol{A}\boldsymbol{x} + \boldsymbol{B}\boldsymbol{u} \tag{51}$$

where

$$\boldsymbol{A} = -\boldsymbol{I}_D^{-1} \boldsymbol{g}_L,\ \boldsymbol{B} = \boldsymbol{I}_D^{-1} \boldsymbol{g}_T,\ \boldsymbol{u} = \boldsymbol{T}_D$$

3.4.2 Reverse power flow

The system of equation (40) can be slightly changed if consider the torques T_1, T_2 as driving and T_3 as resisting. The general structure of equation (49) is unchangeable with only difference in $\boldsymbol{\eta}_M$

$$\boldsymbol{\eta}_M = \begin{pmatrix} \dfrac{1}{\eta_{0B}} & -\eta_{1G} & -\eta_{2G} \\ 0 & 1 & 0 \\ 0 & 0 & 1 \\ -\eta_{FG} & 0 & 0 \\ 0 & 1 & -1 \end{pmatrix} \tag{52}$$

Note that $\boldsymbol{\eta}_L$ in this variant does not depend on power direction, unlike variant 1.

3.5 Simulation and testing

3.5.1 Simulink model

The model depicted in Figure 2 conditionally consists of data blocks, a state-space model, and integration. All the information (Table 1) about the mechanism physical parameters is preliminary set to the structure variable *SDms*. All the matrices $\boldsymbol{A}, \boldsymbol{B}$ derived above are stored numerically to reduce excessive computations. The *Torques* block generates external moments according to the numbered shafts in the icon. These values compose a column vector by the block *Vector Concatenate*. The mechanism data and the torque vector are sent to the *Bus* block, where the dynamic variables are updated in the corresponding fields of *SDms* structure. The block *System of Differential Equations* reads

the bus data and computes three bus signals to be sent as field values of the output bus structure. The signal <*AngularSpeeds*> contains the vector of all the rotational velocities as by equation (1). The signal <*PowerDirection*> shows a strategy of choosing the inertial and efficiency matrices. Thus, the value "*1* means direct power flow, *-1* – the reverse one. The signal <*Derivatives*> of the Bus Selector delivers two angular accelerations of side gears to be integrated into the Integrator block with the initial condition W_0. The integrated values are the new angular speed values to be sent back to the input bus to update the *SDms* structure's corresponding fields.

As an example, consider the mechanism operating under the action of external torques T_1, T_2, T_3 in such a way that the carrier torque T_0 is opposite to the sum of the side gear torques T_1, T_2 but does not equal it exactly (Figure 3). The torques T_1 and T_2 work in the same phases with some difference in the modules to reveal the redistribution of power flows for the most general case. Since the final drive ratio is negative, the signs of three input torques coincide. Thus, each shaft may be leading and driven during the simulation time, which is demonstrated in the bottom graphic of the power flow index.

Figure 2 Simulink model of functioning the symmetric DM (see online version for colours)

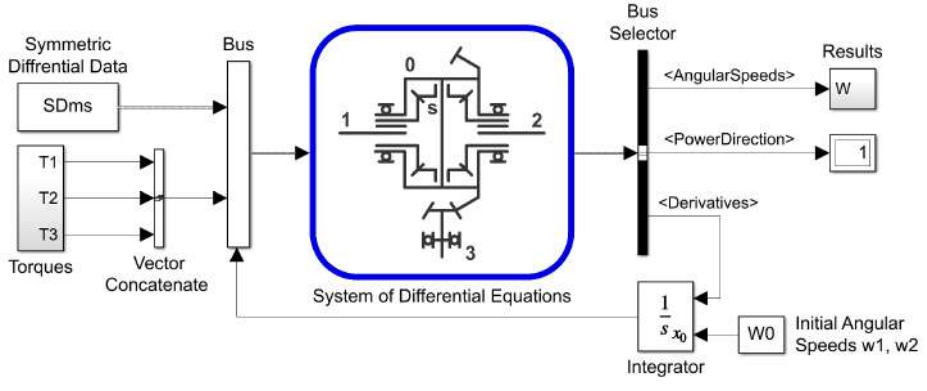

Table 1 Input data for simulating the symmetric differential

Name	*Value*	*Name*	*Value*	*Name*	*Value*	*Name*	*Value*	*Name*	*Value*	*Name*	*Value*
g_F	3.517	I_0, $[kg\,m^2]$	0.1	I_3, $[kg\,m^2]$	1.56×10^{-4}	η_{1G}	0.99	η_{0B}	0.995	l_2, $\left[\frac{Nms}{rad}\right]$	1×10^{-3}
g_{2s}	0.5	I_1, $[kg\,m^2]$	1.8×10^{-4}	I_s, $[kg\,m^2]$	4.0×10^{-5}	η_{2G}	0.99	l_0, $\left[\frac{Nms}{rad}\right]$	5×10^{-3}	l_3, $\left[\frac{Nms}{rad}\right]$	1×10^{-3}
n_s	2	I_2, $[kg\,m^2]$	1.8×10^{-4}	η_{3B}	0.995	η_{FG}	0.975	l_1, $\left[\frac{Nms}{rad}\right]$	1×10^{-3}	l_s, $\left[\frac{Nms}{rad}\right]$	1×10^{-3}

The main result implies redistributing the angular speeds of components. As seen, the side gear shafts' angular speeds are opposite since T_1 has larger module values than T_2

and thus ω_2 becomes counter-rotating owing to an insignificant difference in the carrier's and side gears' torques. Nevertheless, the carrier angular speed also changes phases according to the direction of power flow, with some delays caused by inertial and viscous resistance.

3.5.2 Validation of model variants

The proposed model variants are expected to ensure close computations at the same input dataset. The two model variants (Figure 4) receive the same torque vector signal. The output **V** of each block is the vector of angular speeds combined with the power direction index. The relative errors across rows of the column-vector signal are determined as quotients of differences relative to the outputs of variant 1. The block *RMS* computes the root mean square for estimating an average tendency of difference between model variants. Simulations show that signals from these models are almost identical, with a slight alternating delay in switching the power flow.

Figure 3 Results of simulating the symmetric DM: (a) external load; (b) angular speeds of elements and (c) power flow direction (see online version for colours)

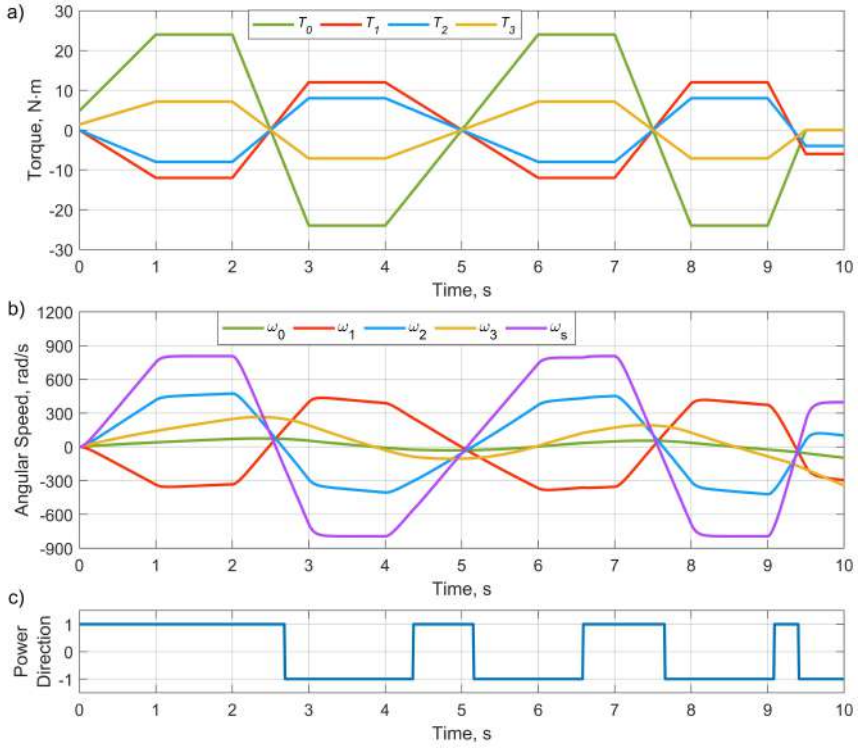

Thus, these two modelling variants can be marked as equivalent by results. On the other hand, variant 1 requires only matrix dimensions 2×2, whereas variant 2 is based on the array with *8×8* dimensions. Consequently, variant 1 ensures a bit better tolerance and stability since some imprecision is accumulated owing to the matrix $\boldsymbol{I}_D$ inversion.

Nevertheless, variant 2 provides a universal technique in deriving state-space equations for mechanical systems and simultaneously determines internal loadings.

Figure 4 Comparison of two model variants by R-square of the relative error

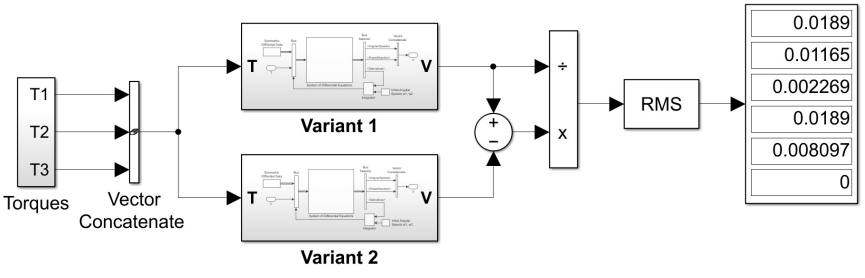

The simulation model proposed was also compared with an *Open Differential* block from the Simulink library. Despite the different approaches in the mechanism modelling, they reflect the close operating tendencies and may fit upon results after being preliminarily adjusted. The main discrepancy is stipulated by neglecting the satellites in the block from the Simulink standard library. The model proposed considers the number of satellites and their gear ratio influencing the moment of inertia reduced to a side gear. Thus, the viscous losses across all the mechanism components affect each other. This model will be considered the basis for evaluating more complex differential mechanisms with asymmetric and controllable torque redistribution.

4 Inter-axle self-locking asymmetric (limited slip) differential

4.1 Differential description

This type belongs to LSDs. The primary asymmetry is organised by the different contact radii of the output shafts' crown gears (Figure 5), which provides an initial torque distribution as 40/60 by the gearing only, Audi technology portal (2021), Audi Quattro (2021). Thus, when a load on the rear axle driveshaft is 60% of the carrier torque and on the front axle drive shaft 40%, both output shafts rotate with the same angular speed. Each crown gear has a set of clutches, the counter-bodies connected to the differential housing (carrier). With the relative rotation of the carrier and crown gears, the friction pairs of the clutches generate forces that reduce or increase the moments on output shafts. The clutch pack can be installed with pre-compression, setting the static friction torque due to the pressing washers. With a decrease of resistance on one of the shafts, its angular speed becomes greater than the carrier angular speed. The excessive power flow from an outrunning shaft returns to the carrier by friction forces, increasing the torque on a lagging shaft. A feature of this design is the dynamic redistribution of friction moments due to the axial component of the gearing reaction. The greater the satellite's force, the greater the compression, and in turn, the greater moment can be passed by friction clutches.

Figure 5 Asymmetric self-locking inter-axle DM with proportional friction moments: (a) design; (b) scheme and (c) proportional action between satellites and crown gears (see online version for colours)

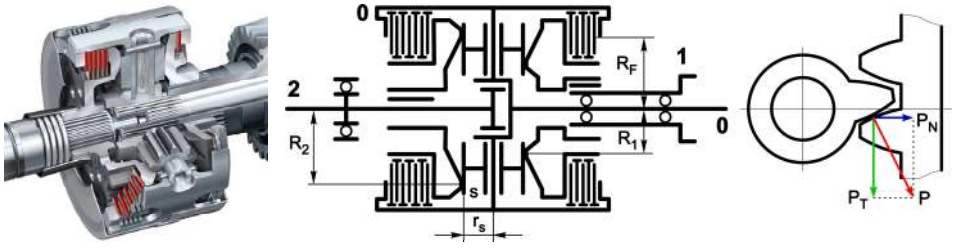

(a) (b) (c)

4.2 Differential's kinematics

Using expressions represented in equations (3) and (4), the general kinematic relations for the asymmetric differential depicted in Figure 5(b), may be reflected as follows

$$\omega_0 = \frac{\omega_1 + g_{12}\omega_2}{1+g_{12}},\ \omega_s = \frac{\omega_1^{(0)}}{i_{1s}^{(0)}} = -\frac{\omega_1 - \omega_0}{g_{1s}} = \frac{\omega_2^{(0)}}{i_{2s}^{(0)}} = \frac{\omega_1 - \omega_0}{g_{2s}},\ \omega_s = \frac{\omega_2 - \omega_1}{g_{2s}(1+g_{12})} \tag{53}$$

where $i_{12}^{(0)} = -g_{12} = \omega_1^{(0)} / \omega_2^{(0)}$ – kinematic ratio and $g_{12} = R_2 / R_1 = 60/40 = 3/2$ – algebraic ratio from axle 1 to axle 2, considering the fact of changing output rotational direction through the mediation of satellites; $g_{2s} = 10/24$ – teeth quotient of the satellite and gear of shaft 2.

Denote $\boldsymbol{\omega}_D$ as the vector of the differential elements' angular speeds and $\boldsymbol{\omega}_H$ as the vector of the counter bodies angular speeds. The matrix $\boldsymbol{g}_D$ represents equation (53) for expressing all the angular speeds through $\boldsymbol{\omega}_D$

$$\boldsymbol{\omega}_D = \begin{pmatrix} \omega_1 \\ \omega_2 \end{pmatrix},\ \boldsymbol{\omega} = \begin{pmatrix} \omega_0 \\ \omega_1 \\ \omega_2 \\ \omega_s \end{pmatrix},\ \boldsymbol{\omega}_H = \begin{pmatrix} 0 \\ \omega_0 \\ 0 \\ 0 \end{pmatrix},\ \boldsymbol{g}_D = \begin{pmatrix} \frac{1}{1+g_{12}} & \frac{g_{12}}{1+g_{12}} \\ 1 & 0 \\ 0 & 1 \\ \frac{-1}{g_{2s}(1+g_{12})} & \frac{1}{g_{2s}(1+g_{12})} \end{pmatrix},$$

$$\boldsymbol{\omega} = \boldsymbol{\omega}_D \boldsymbol{g}_D \tag{54}$$

4.3 Friction moment

In this design, the friction forces appeared due to the relative sliding in the clutches between the friction discs, some of which are tied with an output gear and others with the carrier body. As shown in Figure 5(c), the radial (axial) compressive force P_N is proportional to the tangential force P_T based on the gearing contact angle. The gears of shafts 1 and 2 are a bit movable along slot junctions, which is enough for compensating

the clutches' compliances and increasing mechanical pressure between friction couples. The friction moment must be limited in order, on the one hand, to ensure the redistribution of moments, avoiding excessive clutch locking, and on the other hand, to prevent the reduction of DM efficiency, additional loads on the driving shafts, and increase of tyres' slip as well. Suppose that the static frictional moment is preset by the preliminary adjusted tightening of the carrier body's washers in this design. For each $k = 1,2$ shaft's clutch, the friction moment is modelled by

$$F_k = n_s P_{Nk} n_{Fk} R_{Fk} \mu_{Fk} = n_s P_{Nk} R_k \frac{R_{Fk}}{R_k} n_{Fk} \mu_{Fk} = n_s P_{Nk} R_k f_k \tag{55}$$

where n_s – number of satellites, P_{Nk} – axial gearing force, n_{Fk} – number of friction couples, R_{Fk} – average friction radius, μ_{Fk} – friction coefficient, $f_k = n_{Fk} \mu_{Fk} R_{Fk} / R_k$ – friction factor.

The friction moments may be expressed directly through side gear moments if the friction is split into static and dynamic components

$$F_k = F_{kd} + F_{ks} = \left| n_s P_k R_k \right| \tan(\alpha) f_k + n_s N_k R_k f_k \tag{56}$$

where F_{kd}, F_{ks} – dynamic and static friction moments, correspondingly, α – gearing angle, N_k – preliminary established axial compression.

The axial component P_N of the gearing contact reaction P does not depend on the direction of the shaft rotation nor the direction of the tangential component P_T (P_k). Thus, the friction moment's dynamic part is written as

$$F_{kd} = n_s P_k R_k \operatorname{sgn}\left(n_s P_k R_k\right) \tan(\alpha) f_k \tag{57}$$

where $\operatorname{sgn}(\cdot)$ – sign function.

The last circumstance imposes nonlinearity on the system of equations. A hyperbolic function can be chosen as a friction model, which ensures the change of slipping sign and rapidly asymptotically approaches one. This prevents the sticking effect leading to a stiff system of equations and, consequently, to the increase in the solution time, and avoids abrupt jerks when the friction moment changes its sign. For $k = 1,2$

$$\mu_{Fk} = \mu_k \tanh\left(c_{fk} \left(\omega_k - \omega_0\right)\right) \tag{58}$$

where μ_k – module value of friction coefficient, c_{fk} – intensity coefficient.

4.4 Differential's dynamics

Depending on the relation of external power flows on the differential's shafts, two systems of equations can describe the dynamics of such a mechanism configuration (Figure 5). In the case of direct power flow (the carrier is driving)

$$\begin{cases} I_0\varepsilon_0 = T_0 - \dfrac{M_1}{\eta_{0B}} - \dfrac{M_2}{\eta_{0B}} - \dfrac{L_0}{\eta_{0B}} + \dfrac{L_1}{\eta_{0B}} + \dfrac{L_2}{\eta_{0B}} + \dfrac{F_1}{\eta_{0B}} + \dfrac{F_2}{\eta_{0B}} \\ I_1\varepsilon_1 = M_1\eta_{1G} - L_1 - F_1 + T_1 \\ I_2\varepsilon_2 = M_2\eta_{2G} - L_2 - F_2 + T_2 \\ \dfrac{n_s I_s}{g_{2s}}\varepsilon_s = M_1 g_{12} - M_2 - \dfrac{n_s L_s}{g_{2s}} \end{cases} \quad (59)$$

where $M_k = n_s P_k R_k$ – moment of contact forces between satellites and crown gear; other symbols correspond to designations made above, $k = 1,2$.

In the case of reverse power flow (output shafts are driving)

$$\begin{cases} I_0\varepsilon_0 = M_1\eta_{1G} + M_2\eta_{2G} - \dfrac{L_0}{\eta_{0B}} + \dfrac{L_1}{\eta_{0B}} + \dfrac{L_2}{\eta_{0B}} + \dfrac{F_1}{\eta_{0B}} + \dfrac{F_2}{\eta_{0B}} + \dfrac{T_0}{\eta_{0B}} \\ I_1\varepsilon_1 = T_1 - L_1 - F_1 - M_1 \\ I_2\varepsilon_2 = T_2 - L_2 - F_2 - M_2 \\ \dfrac{n_s I_s}{g_{2s}}\varepsilon_s = M_2\eta_{2G} n_s - M_1\eta_{1G} g_{12} - \dfrac{n_s L_s}{g_{2s}} \end{cases} \quad (60)$$

The number of equations is less than the quantity of unknown variables, including M_k and nonlinearity due to sign function in friction moments. Thus, three variants of solving this problem are proposed. Variant 1 is based on the technique described in variant 1 of symmetric differential. Variant 2 is based on an extension of variant 1 and a method that allows the gearing moments into the system of equations as unknown parameters to be determined simultaneously with angular accelerations. Nevertheless, this variant requires solving a nonlinear system of equations due to the uncertainty of the vector $\boldsymbol{M}$ signs. Variant 3 combines variant 2 for symmetric differential and variant 2 for the differential with proportional friction moments. It uses the systems of equations (59) and (60) without changes, requiring two additional equations of kinematic constraints.

4.5 Proposed variant 1

4.5.1 Direct power flow

The second and third equations of equations (59) and (60) are to be substituted into the upper and lower equations, eliminating unknown M_k. Thus, the components for equations of the carrier and satellite equilibriums in the case of direct power flow are

$$I_{\Sigma 1} = \frac{I_0}{1+g_{12}} + \frac{I_1}{\eta_{1G}\eta_{0B}},\ I_{2\Sigma} = \frac{I_0 g_{12}}{1+g_{12}} + \frac{I_2}{\eta_{2G}\eta_{0B}},\ F_\Sigma = \frac{\eta_{1L}}{\eta_{0B}}F_1 + \frac{\eta_{2L}}{\eta_{0B}}F_2, \quad (61)$$

$$T_\Sigma = T_0 + \frac{T_1}{\eta_{1G}\eta_{0B}} + \frac{T_2}{\eta_{2G}\eta_{0B}},\ L_\Sigma = \frac{L_0}{\eta_{0B}} + \frac{\eta_{1L}}{\eta_{0B}}L_1 + \frac{\eta_{2L}}{\eta_{0B}}L_2$$

$$I_{1s} = \frac{I_1 g_{12}}{\eta_{1G}} + \frac{n_s I_s}{g_{2s}^2 (1+g_{12})}\ ,\ I_{2s} = \frac{I_2}{\eta_{2G}} + \frac{n_s I_s}{g_{2s}^2 (1+g_{12})}\ , \tag{62}$$

$$T_S = -\frac{T_1 g_{12}}{\eta_{1G}} + \frac{T_2}{\eta_{2G}}\ ,\ F_S = \frac{F_2}{\eta_{2G}} - \frac{F_1 g_{12}}{\eta_{1G}}\ ,\ L_S = \frac{L_2}{\eta_{2G}} - \frac{g_{12}}{\eta_{1G}} L_1 + \frac{n_s}{g_{2s}} L_s$$

where $\eta_{kL} = 1/\eta_{kG} - 1$ for $k = 1,2$.

Denote the vectors and matrices as

$$\boldsymbol{I}_D = \begin{pmatrix} I_{\Sigma 1} & I_{2\Sigma} \\ -I_{1S} & I_{2S} \end{pmatrix},\ \boldsymbol{T}_D = \begin{pmatrix} T_\Sigma \\ T_S \end{pmatrix},\ \boldsymbol{F}_D = \begin{pmatrix} F_\Sigma \\ F_S \end{pmatrix},\ \boldsymbol{L}_D = \begin{pmatrix} L_\Sigma \\ L_S \end{pmatrix},\ \boldsymbol{F} = \begin{pmatrix} F_1 \\ F_2 \end{pmatrix},\ \boldsymbol{M} = \begin{pmatrix} M_1 \\ M_2 \end{pmatrix},$$
$$\boldsymbol{I}_G = \begin{pmatrix} I_1 & 0 \\ 0 & I_2 \end{pmatrix}$$

$$\boldsymbol{T} = \begin{pmatrix} T_0 \\ T_1 \\ T_2 \end{pmatrix},\ \boldsymbol{L} = \begin{pmatrix} L_0 \\ L_1 \\ L_2 \\ L_s \end{pmatrix},\ \boldsymbol{f} = \begin{pmatrix} f_1 \\ f_2 \end{pmatrix},\ \boldsymbol{\eta}_G = \begin{pmatrix} \eta_{1G} \\ \eta_{2G} \end{pmatrix},\ \boldsymbol{T}_G = \begin{pmatrix} T_1 \\ T_2 \end{pmatrix},\ \boldsymbol{R} = \begin{pmatrix} R_1 \\ R_2 \end{pmatrix},\ \boldsymbol{N} = \begin{pmatrix} N_1 \\ N_2 \end{pmatrix}, \tag{63}$$

$$\boldsymbol{\eta}_T = \begin{pmatrix} 1 & \frac{1}{\eta_{1G}\eta_{0B}} & \frac{1}{\eta_{2G}\eta_{0B}} \\ 0 & -\frac{g_{12}}{\eta_{1G}} & \frac{1}{\eta_{2G}} \end{pmatrix},\ \boldsymbol{\eta}_L = \begin{pmatrix} \frac{1}{\eta_{0B}} & \frac{\eta_{1L}}{\eta_{0B}} & \frac{\eta_{2L}}{\eta_{0B}} & 0 \\ 0 & -\frac{g_{12}}{\eta_{1G}} & \frac{1}{\eta_{2G}} & \frac{n_s}{g_{2s}} \end{pmatrix},\ \boldsymbol{\eta}_F = \begin{pmatrix} \frac{\eta_{1L}}{\eta_{0B}} & \frac{\eta_{2L}}{\eta_{0B}} \\ -\frac{g_{12}}{\eta_{1G}} & \frac{1}{\eta_{2G}} \end{pmatrix}$$

Then, the major relations between the vectors can be written as

$$\boldsymbol{T}_D = \boldsymbol{\eta}_T \boldsymbol{T}\ ,\ \boldsymbol{L}_D = \boldsymbol{\eta}_L \boldsymbol{L}\ ,\ \boldsymbol{F}_D = \boldsymbol{\eta}_F \boldsymbol{F} \tag{64}$$

The vector $\boldsymbol{L}$ of viscous loss may be expressed using equations (31) and (54)

$$\boldsymbol{L} = \boldsymbol{l}\left(\boldsymbol{\omega} - \boldsymbol{\omega}_H\right) \tag{65}$$

The vector of friction moment and its components are calculated as

$$\boldsymbol{F} = \boldsymbol{F}_d + \boldsymbol{F}_s = diag\left(\boldsymbol{f}\right) diag\left(sgn\left(\boldsymbol{M}\right)\right) \boldsymbol{M} \tan\left(\alpha\right) + diag\left(\boldsymbol{f}\right) diag\left(\boldsymbol{R}\right) \boldsymbol{N} n_s \tag{66}$$

Accepting the form of the system derived in equation (33), obtain the matrix equation

$$\boldsymbol{\varepsilon}_D = \boldsymbol{I}_D^{-1}\left(\boldsymbol{T}_D - \boldsymbol{F}_D - \boldsymbol{L}_D\right) \tag{67}$$

The vector $\boldsymbol{M}$ of gearing moments remains undetermined at the current solution step. Consequently, it can be obtained from the preceding step, assuming insignificant changes during a time increment.

$$\boldsymbol{M} = \left(diag\left(\boldsymbol{\eta}_G\right)\right)^{-1}\left(\boldsymbol{I}_G \boldsymbol{\varepsilon}_D + \boldsymbol{L} + \boldsymbol{F} - \boldsymbol{T}_G\right) \tag{68}$$

4.5.2 Reverse power flow

Keeping the same structure for basic equations from the case of direct flow, only those components that change values depending on power direction are reflected below:

$$I_{\Sigma 1} = \frac{I_0}{1+g_{12}} + I_1\eta_{1G}\,,\; I_{2\Sigma} = \frac{I_0 g_{12}}{1+g_{12}} + I_2\eta_{2G}\,, \tag{69}$$

$$I_{1s} = I_1\eta_{1G}g_{12} + \frac{n_s I_s}{g_{2s}^2\left(1+g_{12}\right)}\;,\; I_{2s} = I_2\eta_{2G} + \frac{n_s I_s}{g_{2s}^2\left(1+g_{12}\right)}\;,$$

$$\boldsymbol{\eta}_T = \begin{pmatrix} \dfrac{1}{\eta_{0B}} & \eta_{1G} & \eta_{2G} \\ 0 & -g_{12}\eta_{1G} & \eta_{2G} \end{pmatrix},\; \boldsymbol{\eta}_L = \begin{pmatrix} \dfrac{1}{\eta_{0B}} & \dfrac{\eta_{1L}}{\eta_{0B}} & \dfrac{\eta_{2L}}{\eta_{0B}} & 0 \\ 0 & -g_{12}\eta_{1G} & \eta_{2G} & \dfrac{n_s}{g_{2s}} \end{pmatrix},$$

$$\boldsymbol{\eta}_F = \begin{pmatrix} \dfrac{\eta_{1L}}{\eta_{0B}} & \dfrac{\eta_{2L}}{\eta_{0B}} \\ -g_{12}\eta_{1G} & \eta_{2G} \end{pmatrix}$$

where $\eta_{kL} = \eta_{kG}\eta_{0B} - 1$ for $k = 1,2$.

The matrix equation for determining the vector $\boldsymbol{M}$ becomes more simple

$$\boldsymbol{M} = \boldsymbol{T}_G - \boldsymbol{I}_G\boldsymbol{\varepsilon}_D - \boldsymbol{L} - \boldsymbol{F} \tag{70}$$

Thus, this variant is based on a slight delay in vector $\boldsymbol{M}$ values but ensures quick computations and linearity of the equation system.

4.6 Proposed variant 2

4.6.1 Direct power flow

The structure of system equation (24) may be completed with two equations for shafts 1 and 2 from equation (59), preventing linear combinations. The needed vectors are as follows

$$\dot{\boldsymbol{x}} = \begin{pmatrix} \varepsilon_1 \\ \varepsilon_2 \\ M_1 \\ M_2 \end{pmatrix} = \begin{pmatrix} \boldsymbol{\varepsilon}_D \\ \boldsymbol{M} \end{pmatrix},\; \boldsymbol{F}_{Dd} = \begin{pmatrix} F_{\Sigma d} \\ F_{Sd} \\ F_{1d} \\ F_{2d} \end{pmatrix},\; \boldsymbol{F}_{Ds} = \begin{pmatrix} F_{\Sigma s} \\ F_{Ss} \\ F_{1s} \\ F_{2s} \end{pmatrix},\; \boldsymbol{T}_D = \begin{pmatrix} T_\Sigma \\ T_S \\ T_1 \\ T_2 \end{pmatrix},\; \boldsymbol{L}_D = \begin{pmatrix} L_\Sigma \\ L_S \\ L_1 \\ L_2 \end{pmatrix},$$

$$\boldsymbol{f}_Z = \begin{pmatrix} \boldsymbol{Z}_{2,1} \\ \boldsymbol{f} \end{pmatrix} \tag{71}$$

where $\dot{\boldsymbol{x}}$ – vector of integrated variables, $\boldsymbol{F}_{Dd}$, $\boldsymbol{F}_{Ds}$ – vectors of dynamic and static friction components, $\boldsymbol{Z}_{2,1}$ – zero vector with two rows.

These vectors may be decomposed, by introducing matrices, as

$$\boldsymbol{\eta}_T = \begin{pmatrix} 1 & \dfrac{1}{\eta_{1G}\eta_{0B}} & \dfrac{1}{\eta_{2G}\eta_{0B}} \\ 0 & -g_{12}/\eta_{1G} & 1/\eta_{2G} \\ 0 & 1 & 0 \\ 0 & 0 & 1 \end{pmatrix}, \ \boldsymbol{\eta}_L = \begin{pmatrix} \dfrac{1}{\eta_{0B}} & \dfrac{\eta_{1L}}{\eta_{0B}} & \dfrac{\eta_{2L}}{\eta_{0B}} & 0 \\ 0 & \dfrac{-g_{12}}{\eta_{1G}} & \dfrac{1}{\eta_{2G}} & \dfrac{n_s}{g_{2s}} \\ 0 & 1 & 0 & 0 \\ 0 & 0 & 1 & 0 \end{pmatrix},$$

$$\boldsymbol{\eta}_F = \begin{pmatrix} \dfrac{\eta_{1L}}{\eta_{0B}} & \dfrac{\eta_{2L}}{\eta_{0B}} \\ -\dfrac{g_{12}}{\eta_{1G}} & \dfrac{1}{\eta_{2G}} \\ 1 & 0 \\ 0 & 1 \end{pmatrix} \tag{72}$$

where $\eta_{kL} = 1/\eta_{kG} - 1$ for $k = 1,2$.

The new block matrices representing influences of all the variables are formed using equations (63) and (72) as

$$\boldsymbol{G}_D = \begin{pmatrix} \boldsymbol{I}_D & \boldsymbol{Z}_{2,2} \\ \boldsymbol{I}_G & -diag(\boldsymbol{\eta}_G) \end{pmatrix}, \ \boldsymbol{H}_F = \begin{pmatrix} \boldsymbol{Z}_{4,2} & \boldsymbol{\eta}_F \end{pmatrix} \tag{73}$$

where $\boldsymbol{Z}_{2,2}$ and $\boldsymbol{Z}_{4,2}$ – zero matrices with *2×2* and *4×2* dimensions, respectively; other components correspond to those represented in equation (63). Then, the components of the equation system may be compactly rewritten in matrix form as

$$\boldsymbol{T}_D = \boldsymbol{\eta}_T \boldsymbol{T}, \ \boldsymbol{L}_D = \boldsymbol{\eta}_L \boldsymbol{L}, \ \boldsymbol{F}_{Ds} = \boldsymbol{\eta}_F diag(\boldsymbol{f}) diag(\boldsymbol{R}) \boldsymbol{N} n_s, \tag{74}$$

$$\boldsymbol{F}_{Dd} = \boldsymbol{H}_F diag(\boldsymbol{f}_Z) diag(sgn(\dot{\boldsymbol{x}})) \dot{\boldsymbol{x}} \tan(\alpha) = \boldsymbol{F}_{Dd}(\dot{\boldsymbol{x}})$$

where the vector $\boldsymbol{L}$ of viscous losses is calculated in the same way as in equation (65).

Finally, the matrix equation of equilibrium may be written in the form of a nonlinear objective as

$$\boldsymbol{G}_D \dot{\boldsymbol{x}} + \boldsymbol{F}_{Dd}(\dot{\boldsymbol{x}}) + \boldsymbol{F}_{Ds} + \boldsymbol{L}_D - \boldsymbol{T}_D = \boldsymbol{Z}_{4,1} \tag{75}$$

where $\boldsymbol{Z}_{4,1}$ – zero column-vector with 4 elements.

4.6.2 Reverse power flow

The inertial matrix $\boldsymbol{I}_D$ is entirely identical to the reverse case of variant 1. The minor difference in math model compared to the case of direct flow consists of matrices given by

$$\boldsymbol{\eta}_T = \begin{pmatrix} \dfrac{1}{\eta_{0B}} & \eta_{1G} & \eta_{2G} \\ 0 & -g_{12}\eta_{1G} & \eta_{2G} \\ 0 & 1 & 0 \\ 0 & 0 & 1 \end{pmatrix}, \quad \boldsymbol{\eta}_L = \begin{pmatrix} \dfrac{1}{\eta_{0B}} & \dfrac{\eta_{1L}}{\eta_{0B}} & \dfrac{\eta_{2L}}{\eta_{0B}} & 0 \\ 0 & -g_{12}\eta_{1G} & \eta_{2G} & \dfrac{n_s}{g_{2s}} \\ 0 & 1 & 0 & 0 \\ 0 & 0 & 1 & 0 \end{pmatrix},$$

$$\boldsymbol{\eta}_F = \begin{pmatrix} \dfrac{\eta_{1L}}{\eta_{0B}} & \dfrac{\eta_{2L}}{\eta_{0B}} \\ -g_{12}\eta_{1G} & \eta_{2G} \\ 1 & 0 \\ 0 & 1 \end{pmatrix} \tag{76}$$

where $\eta_{kL} = \eta_{kG}\eta_{0B} - 1$ for $k = 1,2$. The matrix of variables' influence also changes one block element

$$\boldsymbol{G}_D = \begin{pmatrix} \boldsymbol{I}_D & \boldsymbol{Z}_{2,2} \\ \boldsymbol{I}_G & \boldsymbol{E}_{2,2} \end{pmatrix} \tag{77}$$

where $\boldsymbol{E}_{2,2}$ – diagonal identity matrix with *2×2* dimension.

4.7 Proposed variant 3

4.7.1 Direct power flow

The system of equations (59) and (60) may be reorganised with matrix form. The vectors representing kinematic, physical, and force parameters are:

$$\boldsymbol{\varepsilon} = \begin{pmatrix} \varepsilon_0 \\ \varepsilon_1 \\ \varepsilon_2 \\ \varepsilon_s \end{pmatrix}, \ \boldsymbol{I} = \begin{pmatrix} I_0 \\ I_1 \\ I_2 \\ I_s \end{pmatrix}, \ \boldsymbol{T} = \begin{pmatrix} T_0 \\ T_1 \\ T_2 \\ 0 \end{pmatrix}, \ \boldsymbol{L} = \begin{pmatrix} L_0 \\ L_1 \\ L_2 \\ L_s \end{pmatrix}, \ \boldsymbol{\omega} = \begin{pmatrix} \omega_0 \\ \omega_1 \\ \omega_2 \\ \omega_s \end{pmatrix}, \ \boldsymbol{g} = \begin{pmatrix} 1 \\ 1 \\ 1 \\ n_s / g_{2s} \end{pmatrix},$$

$$\boldsymbol{F}_d = \begin{pmatrix} F_{1d} \\ F_{2d} \end{pmatrix}, \ \boldsymbol{F}_s = \begin{pmatrix} F_{1s} \\ F_{2s} \end{pmatrix}, \ \boldsymbol{M} = \begin{pmatrix} M_1 \\ M_2 \end{pmatrix}, \ \boldsymbol{f} = \begin{pmatrix} f_1 \\ f_2 \end{pmatrix}, \ \boldsymbol{f}_Z = \begin{pmatrix} \boldsymbol{Z}_{4,1} \\ \boldsymbol{f} \end{pmatrix}, \ \boldsymbol{R} = \begin{pmatrix} R_1 \\ R_2 \end{pmatrix},$$

$$\boldsymbol{N} = \begin{pmatrix} N_1 \\ N_2 \end{pmatrix} \tag{78}$$

where $\boldsymbol{Z}_{4,1}$ – zero vector with 4 rows.

The following matrices reflect the impact of efficiencies and gear ratios

$$\boldsymbol{\eta}_M = \begin{pmatrix} \frac{1}{\eta_{0B}} & \frac{1}{\eta_{0B}} \\ -\eta_{1G} & 0 \\ 0 & -\eta_{2G} \\ -g_{12} & 1 \end{pmatrix}, \ \boldsymbol{\eta}_F = \begin{pmatrix} \frac{-1}{\eta_{0B}} & \frac{-1}{\eta_{0B}} \\ 1 & 0 \\ 0 & 1 \\ 0 & 0 \end{pmatrix}, \ \boldsymbol{\eta}_L = \begin{pmatrix} \frac{1}{\eta_{0B}} & \frac{-1}{\eta_{0B}} & \frac{-1}{\eta_{0B}} & 0 \\ 0 & 1 & 0 & 0 \\ 0 & 0 & 1 & 0 \\ 0 & 0 & 0 & \frac{n_s}{g_{2s}} \end{pmatrix} \tag{79}$$

The kinematic restrictions are expressed with the matrix $\boldsymbol{g}_\omega$ reflecting dependencies from equation (53)

$$\boldsymbol{g}_\omega = \begin{pmatrix} (1+g_{12}) & -1 & -g_{12} & 0 \\ 0 & 1 & -1 & g_{2s}(1+g_{12}) \end{pmatrix} \text{ and } \boldsymbol{g}_\omega \boldsymbol{\varepsilon} = \boldsymbol{Z}_{2,1} \tag{80}$$

where $\boldsymbol{Z}_{2,1}$ – zero vector with two rows.

The block matrix of inertias and kinematic constraint influence can be composed as

$$\boldsymbol{G}_D = \begin{pmatrix} diag(\boldsymbol{I})\, diag(\boldsymbol{g}) & \boldsymbol{\eta}_M \\ \boldsymbol{g}_\omega & \boldsymbol{Z}_{2,2} \end{pmatrix} \tag{81}$$

The static component of friction moment is

$$\boldsymbol{F}_s = diag(\boldsymbol{f})\, diag(\boldsymbol{R})\, \boldsymbol{N} n_s \tag{82}$$

Reducing the matrix $\boldsymbol{\eta}_F$ to the new dimension, considering rows of kinematic equations equation (80), and determining $\boldsymbol{F}_{Ds}$, obtain

$$\boldsymbol{g}_{Fs} = \begin{pmatrix} \boldsymbol{\eta}_F \\ \boldsymbol{Z}_{2,2} \end{pmatrix}, \ \boldsymbol{F}_{Ds} = \boldsymbol{g}_{Fs} \boldsymbol{F}_s = \begin{pmatrix} \boldsymbol{\eta}_F \\ \boldsymbol{Z}_{2,2} \end{pmatrix} diag(\boldsymbol{f})\, diag(\boldsymbol{R})\, \boldsymbol{N} n_s \tag{83}$$

Combining vectors of unknowns, states, and external load, get

$$\dot{\boldsymbol{x}} = \begin{pmatrix} \boldsymbol{\varepsilon} \\ \boldsymbol{M} \end{pmatrix}, \ \boldsymbol{x} = \begin{pmatrix} \boldsymbol{\omega} \\ \boldsymbol{K} \end{pmatrix}, \ \boldsymbol{T}_D = \begin{pmatrix} \boldsymbol{T} \\ \boldsymbol{Z}_{2,1} \end{pmatrix} \tag{84}$$

where $\boldsymbol{K}$ – vector of internal moments' integral.

The dynamic component of friction moment can be expressed using $\dot{\boldsymbol{x}}$. Denote,

$$\boldsymbol{g}_{Fd} = \tan(\alpha) \begin{pmatrix} \boldsymbol{Z}_{4,4} & \boldsymbol{\eta}_F \\ \boldsymbol{Z}_{2,4} & \boldsymbol{Z}_{2,2} \end{pmatrix} \boldsymbol{f}_Z\, diag\left(sgn(\dot{\boldsymbol{x}})\right), \text{ then } \boldsymbol{F}_{Dd} = \boldsymbol{g}_{Fd} \dot{\boldsymbol{x}} \tag{85}$$

where $\boldsymbol{Z}_{m,n}$ – zero matrix of $m \times n$ dimension.

Introducing vectors and matrices for computing viscous losses, they can be derived as

$$\boldsymbol{l}=\begin{pmatrix} \\ l_0 \\ l_1 \\ l_2 \\ l_s \end{pmatrix},\ \boldsymbol{e}_\omega=\begin{pmatrix} 1 & 0 & 0 & 0 \\ -1 & 1 & 0 & 0 \\ 0 & 0 & 1 & 0 \\ 0 & 0 & 0 & 1 \end{pmatrix},\ \boldsymbol{L}=diag\left(\boldsymbol{l}\right)\boldsymbol{e}_\omega\boldsymbol{\omega},$$

$$\boldsymbol{g}_L=\begin{pmatrix} \boldsymbol{\eta}_L \\ \boldsymbol{Z}_{2,4} \end{pmatrix},\ \boldsymbol{l}_D=diag\left(\boldsymbol{l}\right)\begin{pmatrix} \boldsymbol{e}_\omega & \boldsymbol{Z}_{4,2} \end{pmatrix},\ \boldsymbol{L}_D=\begin{pmatrix} \boldsymbol{\eta}_L\boldsymbol{L} \\ \boldsymbol{Z}_{2,1} \end{pmatrix}=\boldsymbol{g}_L\boldsymbol{l}_D\boldsymbol{x} \tag{86}$$

where $\boldsymbol{l}$ – vector of viscous resistance coefficients, $\boldsymbol{e}_\omega$ – matrix of angular speeds' relativity.

Finally, the matrix system of equations is written as a nonlinear problem as

$$\boldsymbol{G}_D\dot{\boldsymbol{x}}+\boldsymbol{F}_{Dd}+\boldsymbol{F}_{Ds}+\boldsymbol{L}_D-\boldsymbol{T}_D=\boldsymbol{Z}_{6,1} \tag{87}$$

or

$$\left(\boldsymbol{G}_D+\boldsymbol{g}_{Fd}\right)\dot{\boldsymbol{x}}+\boldsymbol{g}_L\boldsymbol{l}_D\boldsymbol{x}+\boldsymbol{g}_{Fs}\boldsymbol{F}_s-\boldsymbol{T}_D=\boldsymbol{Z}_{6,1}$$

4.7.2 Reverse power flow

Only one matrix requires to be replaced if shafts 1 and 2 are driving, namely

$$\boldsymbol{\eta}_M=\begin{pmatrix} \\ -\eta_{1G} & -\eta_{2G} \\ 1 & 0 \\ 0 & 1 \\ g_{12}\eta_{1G} & -\eta_{2G} \end{pmatrix} \tag{88}$$

4.8 Simulation of asymmetric self-Locking DM

All three variants were simulated using the same structure pattern depicted in Figure 2. The main difference with the Simulink-model of self-locking differential (Table 2) in Figure 6 consists of the block *Delay One Step*. In variant 1, this block is connected with the bus output <*InternalMoments*> unlike that shown in Figure 6 for variants 2 and 3. Since variant 1 uses values of internal moments determined on a preceding step, this vector must be looped. For variants 2 and 3, the output vector <*Derivatives*> is looped to deliver the initial solution for iterating the system of nonlinear equations. As at a small-time increment, the answers do not differ significantly, the previous derivatives are stored into the memory for use as an initial approximation for the next step of solving the nonlinear problem. The block *Delay One Step* also has the lower port for passing the initial vector of its state, which is assigned in the structure of the DM data.

Figure 6 Simulink model of functioning the asymmetric self-locking DM with proportional friction moments (see online version for colours)

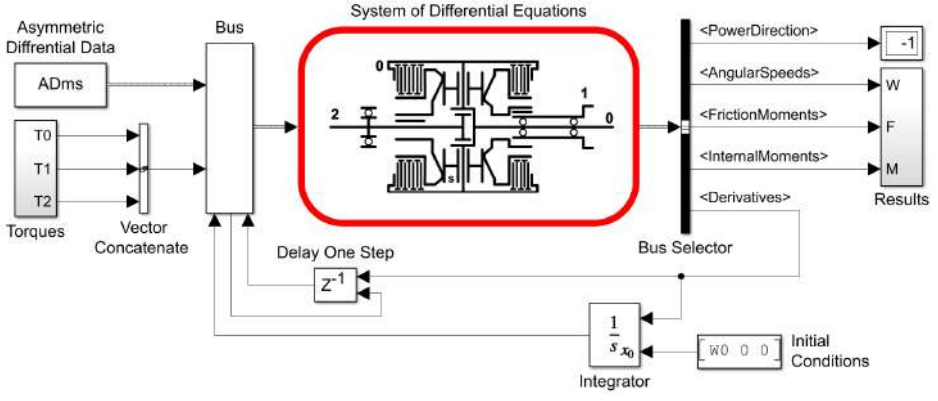

Table 2 Input data for simulating the differential with proportional friction moments

Name	*Value*	*Name*	*Value*	*Name*	*Value*	*Name*	*Value*	*Name*	*Value*	*Name*	*Value*
g_{12}	60/40	I_0, $[kg\,m^2]$	2.9×10^{-2}	I_s, $[kg\,m^2]$	6.0×10^{-5}	η_{1G}	0.99	μ_1, μ_2	0.15	l_1, $\left[\frac{Nms}{rad}\right]$	1×10^{-3}
g_{2s}	10/24	I_1, $[kg\,m^2]$	4.8×10^{-3}	n_{F1}, n_{F2}	1, 9	η_{2G}	0.99	c_{f1}, c_{f2}	4	l_2, $\left[\frac{Nms}{rad}\right]$	1×10^{-3}
n_s	4	I_2, $[kg\,m^2]$	5.8×10^{-3}	α, °	20	η_{0B}	0.995	l_0, $\left[\frac{Nms}{rad}\right]$	5×10^{-3}	l_s, $\left[\frac{Nms}{rad}\right]$	1×10^{-3}

4.8.1 Validation of model variants

Figure 7 shows the modelling results of operating the differential based on variant 2 and comparing absolute differences in angular speeds with variants 1 and 3. Thus, the deviations of the solutions between variants 2 and 1 are estimated using the absolute difference $\Delta\omega_{21}$, and between variants 2 and 3 – $\Delta\omega_{23}$: parts (f) and (g), respectively. In this case, variant 2 was chosen as the fundamental compromise, which includes both elements of the 1st and 2nd variants. Note that, in general, all variants provide solutions that are the closest in form and values. The fewer changes of the power flow direction occur in the given conditions. Thus, for example, comparing the graphs of positions (d) and (g), the power flow from the beginning to 3.5 s remained practically direct, which was reflected by the minimal values of the absolute error $\Delta\omega_{23}$. A critical error at a specific offset in the transition phases determines a further increase in deviations when the power flow direction changes sign. Nevertheless, variants 2 and 3 provide minimal deviation values of internal forces – frictional moments and driving torques on the crown

gears. In contrast, the corresponding data of variant 1 may lag behind in phase the more intensive changes in the load mode on the differential shafts. Nevertheless, the kinematic accuracy of variant 1 is relatively high (Figure 7(f)).

Figure 7 Results of simulating the model of the DM with proportional friction moments: (a) angular speeds; (b) friction and gear moments; (c) load; (d) power flow; (f) absolute errors of angular speeds between variants 2 and 1 and (g) absolute errors of angular speeds between variants 2 and 3 (see online version for colours)

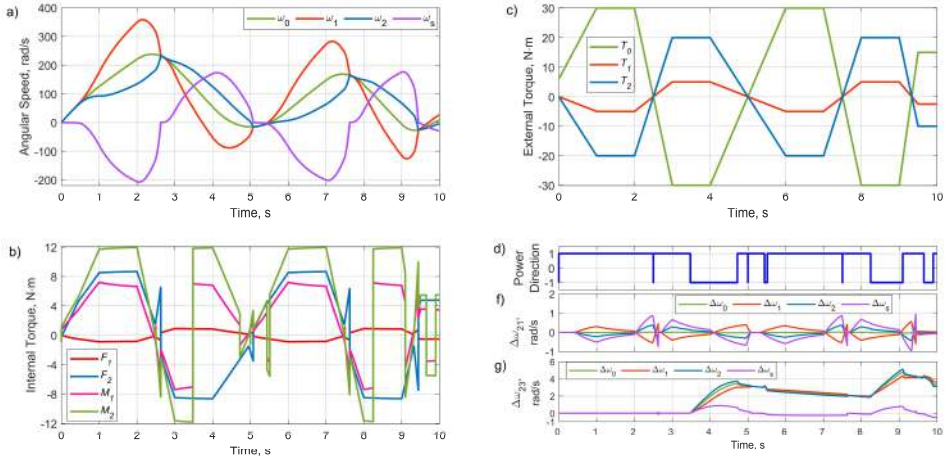

4.8.2 Analysis of mechanism modelling

In contrast to the symmetric DM results, in Figure 7(a), the sections where the curves of carrier's and output shafts' angular speeds coincide are traced, which is caused by the impossibility to overcome the internal friction by external torques. At the same time, the change of external torques' directions (Figure 7(c)) is visibly accompanied by a shift in output shafts' roles, namely outrunning or lagging. Figure 7(b) shows the curves of internal moments on the crown gears M_1, M_2 and in the friction clutches F_1, F_2. Note that the crown gear torques maintain the proportionality preset in equation (53), i.e. the approximate ratio of 40/60. It is also apparent that the friction moment on an outrunning shaft is opposite in sign to its rotational direction. Thus, for example, in the time interval 0 to 2.5 s, the driving torque of shaft 2 crown gear is added with the frictional moment in its friction clutch, and of the shaft 1 – is subtracted, which leads to transmitting more torque through shaft 2. And vice versa, in the range 3.5...4.5 s, the driving torque of shaft 1 crown gear is added up with the friction moment of its friction clutch, and of the shaft 2 – decreases since shaft 1 becomes lagging. Also, note that quasi-periodic curves of angular velocities and internal loads correspond to the quasi-periodic form of external loads on the mechanism shafts, indicating the stable nature of the solutions for all the proposed variants.

Another virtual test may be conducted for estimating the influence of proportional friction by omitting this component in the math model, remaining all the other conditions

accepted for the test in Figure 7. Thus, if $\alpha = 0$, $F_{kd} = 0$ equation (56), assuming the results in Figure 7(a) and (b) as basic, the simulation results of operating the model deprived of the proportional friction moments may be expressed by the absolute differences, which are depicted in Figure 8.

Consequently, the absolute curves of simulation without dynamic friction may be obtained by deducting results in Figure 7(a)–(b) from corresponding results in Figure 8. Thus, the lines F_1, F_2 in Figure 7(b) and the lines ΔF_1, ΔF_2 in Figure 8(b) almost compensate each other, which means no dynamic friction. On the contrary, curves M_1, M_2, and ΔM_1, ΔM_2 give the increase in the module values, implying passing output torques exclusively through the crown gears. This leads to essential growing the angular speeds of DM elements.

Figure 8 Results of comparing the model operating with and without proportional friction influence: (a) for angular speeds and (b) for internal torques (see online version for colours)

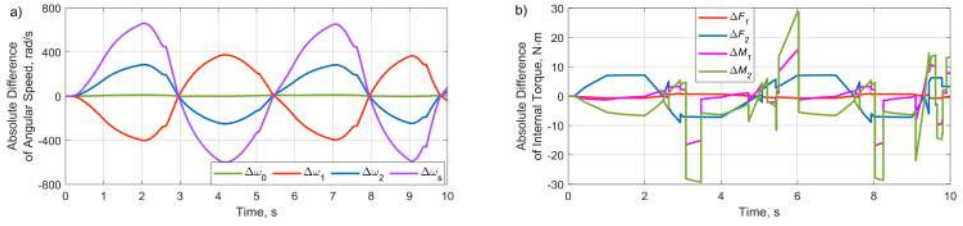

5 Conclusions

The preliminary conclusion of this study indicates that the proposed models fully reflect both the functional purpose and the operating principles of all the considered mechanisms' components. Furthermore, all variants considered within the models of presented mechanism designs are configurable, providing synchronous and very close results estimated with relative and absolute errors.

The choice of model variant depends on the use priorities. Thus, if the main task is obtaining kinematic characteristics at given torque loads on a differential's shafts, then, for symmetric and central differentials, variant 1 can be optimal. In this case, the maximum compactness of the mathematical model and the highest speed of calculations are ensured. Still, it is necessary to recalculate the internal forces if they are needed separately. For example, suppose the differential model is included in the general nonlinear transmission model or is necessary to simultaneously compute the kinematic and dynamic indicators. In that case, it is recommended to use variant 2 for the symmetric differential and variants 2 and 3 for the central differential. In this case, the relative speed of computations decreases, but at the same time, all unknowns are determined.

The Audi Quattro self-locking centre differential model considered in the study has the advantage of versatility owing to simultaneously combining such design features as asymmetry, limited constant friction and proportional dynamic friction depending on resistance moment on a drive crown gear. Other configurations based on this design may be obtained by tuning this model. Comparing the proposed models with the models from

the basic Simulink libraries shows their high relevance. Nevertheless, the elaborated variants have fewer accepted constraints and consider more factors such as the inertia of all elements, efficiency of the mechanical conjunctions, viscous losses, and a change of power flow directions.

Note that despite the clear and adequate results of the virtual validation and simulation of the variants, it is expedient to carry out more comprehensive tests on the functional capabilities, combining the adjustment of a differential's model configuration with a complete simulation of the vehicle transmission and vehicle dynamics models. Such models of differential mechanisms and the modelling approaches, addressing issues of torque vectoring control, including autonomous modes, will be explored in future research.

References

Annicchiarico, C., Rinchi, M., Pellari, S. and Capitani, R. (2014) 'Design of a semi-active differential to improve the vehicle dynamics', *Proceedings of the ASME 2014 12th Biennial Conference on Engineering Systems Design and Analysis. Volume 1*, Copenhagen, Denmark, 25–27 July, V001T02A006, ASME, https://doi.org/10.1115/ESDA2014-20157

Assadian, F., Hancock, M. and Best, M. (2008) *Development of a Control Algorithm for an Active Limited-Slip Differential*, Loughborough University, Conference Contribution, https://hdl.handle.net/2134/8324

Audi Quattro (2021) Internet: https://www.youtube.com/watch?v=mCbVd8mMUJw (Accessed 20 February, 2021).

Audi Technology Portal (2021) Internet: https://www.audi-technology-portal.de/en/drivetrain/quattro_en/crown-gear-differential (Accessed 20 February, 2021).

Brumercik, F., Lukac, M. and Nieoczym, A. (2015) 'Mechanical differential mathematical model. komunikacie', *Communicattions*, Vol. 17, pp.88–91.

Chen, Y-F., Chen, I-M., Chang, J. and Liu, T. (2017a) 'Design and analysis of a new torque vectoring system with a Ravigneaux gearset for vehicle applications', *Energies*, Vol. 10, p.2157, https://doi.org/10.3390/en10122157

Chen, Y-F., Hsu, H-C., Yang, C-P. and Liu, T. (2017b) 'Design and modeling of a novel torque vectoring differential system', *MATEC Web of Conferences*, Vol. 108, p.07004, doi: 10.1051/matecconf/201710807004.

Deur, J., Ivanovic, V., Hancock, M. and Assadian, F. (2010) 'Modeling and analysis of active differential dynamics', *Journal of Dynamic Systems Measurement and Control-Transactions of The ASME*, Vol. 132, p.061501.

Forstinger, M., Bauer, R. and Hofer, A. (2015) 'Modelling and simulation of passive limited-slip differentials', *IFAC-PapersOnLine*, Vol. 48, No. 1, pp.502–507, ISSN 2405-8963, https://doi.org/10.1016/j.ifacol.2015.05.057

Gadola, M. and Chindamo, D. (2018) 'The mechanical limited-slip differential revisited: high-performance and racing car applications', *International Journal of Applied Engineering Research*, Vol. 13, No. 2, pp.1478–1495.

Jaafari, S.M.M. and Shirazi, K.H. (2018) 'Integrated vehicle dynamics control via torque vectoring differential and electronic stability control to improve vehicle handling and stability performance', *J. Dyn. Sys., Meas., Control*, Vol. 140, No. 7, p.071003.

Ji, J., Li, Y.W. and Peng, H. (2011) 'Effects of driveline and tire model on the performance of active differential: modeling and simulation', *Applied Mechanics and Materials*, Vols. 97–98, pp.771–776, Trans Tech Publications, Ltd, https://doi.org/10.4028/www.scientific.net/amm.97-98.771

Mathworks (2021a) Internet: https://www.mathworks.com/help/vdynblks/ref/opendifferential.html (Accessed 21 January, 2021).

Mathworks (2021b) Internet: https://www.mathworks.com/help/vdynblks/ref/limitedslip differential.html (Accessed 5 February, 2021).

Morselli, R., Zanasi, R. and Sandoni, G. (2006) 'Detailed and reduced dynamic models of passive and active limited-slip car differentials', *Mathematical and Computer Modelling of Dynamical Systems*, Vol. 12, No. 4, pp.347–362, doi: 10.1080/13873950500066959.

Russo, R., Strano, S. and Terzo, M. (2016) 'Enhancement of vehicle dynamics via an innovative magnetorheological fluid limited-slip differential', *Mechanical Systems and Signal Processing*, Vol. 70, pp.1193–1208, ISSN 0888-3270, https://doi.org/10.1016/j.ymssp. 2015.09.029

Virlez, G., Brüls, O., Duysinx, P. and Poulet, N. (2011) 'Simulation of differentials in four-wheel drive vehicles using multibody dynamics', *Proceedings of the ASME 2011 International Design Engineering Technical Conferences and Computers and Information in Engineering Conference. Volume 4: 8th International Conference on Multibody Systems, Nonlinear Dynamics, and Control, Parts A and B*, ASME, 28–31 August, 2011, Washington, DC, USA, pp.629–640, https://doi.org/10.1115/DETC2011-48313